PROTON TRANSFER FROM LIGANDS ACTIVATES EXTRANUCLEAR-INITIATED ESTROGEN RECEPTOR SIGNALING

Regla M. Medina-Gali[1,2], Juan Martinez-Pinna[1,3], Laura Marroqui[1,2], Sergio Ciordia[4], Sergi Soriano[1,3], Ricardo Mallavia[1,5], Marina Grimaldi[6], Patrick Balaguer[6] and Angel Nadal[1,2]

[1] Instituto de Investigación, Desarrollo e Innovación en Biotecnología Sanitaria de Elche (IDiBE), Universidad Miguel Hernández de Elche, Elche, Alicante, Spain.

[2] CIBER de Diabetes y Enfermedades Metabólicas Asociadas, Instituto de Salud Carlos III.

[3] Departamento de Fisiología, Genética y Microbiología, Universidad de Alicante, Alicante, Spain.

[4] Functional Proteomics Laboratory, Centro Nacional de Biotecnología-CSIC, Madrid, Spain.

[5] Area of Inorganic Chemistry, Universidad Miguel Hernández de Elche, Elche, Spain.

[6] Institut de Recherche en Cancérologie de Montpellier (IRCM), INSERM U1194, Université Montpellier, Institut Régional du Cancer de Montpellier (ICM), Montpellier, France.

Corresponding author

Angel Nadal, Instituto de Investigación, Desarrollo e Innovación en Biotecnología Sanitaria de Elche (IDiBE), Universidad Miguel Hernández de Elche, 03202-Elche, Alicante, Spain.

E-mail: nadal@umh.es

ABSTRACT

Ligand binding to estrogen receptors (ER), ERα and ERβ, controls the physiology of estrogen-responsive tissues through nuclear and extranuclear initiated pathways. We have found that ligands activate the extranuclear pathway by a mechanism involving proton transfer. The low affinity ligand and widespread endocrine disruptor Bisphenol-A (BPA) initiated nuclear and extranuclear actions. Concentrations similar to the receptor affinity initiated the nuclear pathway, whereas much lower concentrations initiated the extranuclear pathway. Experiments in different cell types using deuterated molecules of BPA and the ERβ agonist, diarylpropionitrile (DPN), indicated that a proton transfer from the hydroxyl groups to an amino acid acceptor within the ligand binding domain switches the extranuclear pathway. Activation of this pathway elicited a pattern of protein interactions with ERβ that regulated most of the important cellular functions. Thus, the extranuclear actions of ERβ are initiated by a molecular mechanism different from that of nuclear actions. This mechanism may work for other ligands and nuclear receptors.

INTRODUCTION

Estrogen receptors alpha (ERα) and beta (ERβ) are involved in the regulation of many physiological processes (*1*). These receptors belong to the ligand-inducible transcription factor superfamily of nuclear receptors (*2*). They activate the so-called nuclear-initiated pathway which regulate gene transcription when the ligand-bound ER acts as a transcription factor (TF) or through the tethered mechanism, in which the ER interacts with other TFs, such as AP-1, Sp1 or NFκB (*3*). In addition, both ER rapidly activate a variety of signaling cascades such as MAKP and AKT that result in significant downstream cellular effects, referred to as the extranuclear-initiated pathway (*4*).

Mice genetically modified to initiate either extranuclear ERα actions (membrane-only estrogen receptor, MOER) or nuclear ERα actions (nuclear-only estrogen receptor, NOER) have demonstrated the existence of different patterns of physiological effects promoted by each pathway (*5-7*). It is of medical interest to find estrogen receptor ligands that uncouple nuclear and extranuclear ER-initiated actions to improve their pharmacological profile. This would avoid unwanted effects in estrogenic drugs used in cancer treatment, hormone replacement therapy or others. For example, Estetrol (E4) is a natural estrogen produced in the human fetal liver during pregnancy that binds to ERα and preferentially activates the nuclear-initiated pathway (*8*). In contrast, the synthetic

estrogens termed "pathway preferential estrogens" (PaPEs) bind both ERα and ERβ and preferentially activate the extranuclear-initiated ER pathway (*9*).

PaPEs retain the essential features of estrogens, such as their geometry and phenolic groups, but have a much lower affinity for the ER. It has been proposed that low affinity is key to selective activation of the extranuclear pathway because these low affinity ligands form an ER-ligand complex that is kinetically stable for a short time but sufficient to activate signaling pathways such as ERK or AKT. However, the ER-ligand complex is not stable for long enough to act as a TF, a process that involves a complex cascade of protein interactions including recruitment of co-regulatory proteins and activation of RNA polymerase (pol) II among others (*9, 10*).
PaPEs share some characteristics with the widespread endocrine disruptor Bisphenol-A (BPA), indeed PaPE-4 is derived from BPA and it retains its core bisphenol structure. BPA is a nonsteroidal estrogen which binds ERα and ERβ proteins but it shows about 1000-fold lower relative binding affinity than 17β-estradiol (E2) and a potency of the transcriptional activity via the nuclear-initiated pathway between 1000 and 10000 lower than E2 (*11, 12*). Studies published along the last two decades indicate that BPA induces effects at doses within the pico- and nanomolar range, in vivo (*13, 14*), ex vivo (*15*) and in vitro (*16*). Experiments using pancreatic β-cells from wild type, ERα and ERβ knockout mice indicate that both receptors are involved in BPA actions via the extranuclear pathway at pico- and nanomolar concentrations (*17, 18*). It is not understood why there is this discrepancy between the affinity of ER for BPA and their potency to cause cellular signaling.

In this work we set out to study how ligand deuteration could modify estrogen receptor affinity and efficacy in activating extranuclear and nuclear pathways. Ligand deuteration is used in drug discovery to modify its efficacy and affinity (*19*). We used different molecules of deuterated BPA and the ERβ-specific ligand DPN. The substitution of hydrogen atoms (^{1}H) with its heavy isotope deuterium (^{2}H), produces subtle changes in the physical and chemical properties of the molecule and keeps its geometry virtually unchanged (*19, 20*). In doing so, we found that the extranuclear effect initiated by ERβ in the presence of BPA was abolished when we used fully deuterated BPA (d_{16}-BPA), but remained unaffected when we used d_{14}-BPA whose hydroxyl groups on the phenols were not deuterated. The same was true when we used the ERβ receptor agonist, DPN,

deuterated at the two hydroxyls (d_2-DPN). According to the kinetic hydrogen isotope effect (*21*), our experiments strongly suggest that the transfer of a proton from hydroxyls in ligands to an acceptor group in the binding site of the receptor is involved in switching the signaling pathway initiated by extranuclear ERβ.

RESULTS

Low affinity ligands trigger the extranuclear pathway with high efficacy

HEK cells transiently transfected with a human ERβ plasmid overexpressed this receptor, its localization being mainly outside the nucleus (Fig. S1A and S1B). Computational docking model shows that E2 forms hydrogen bonds in the ligand-binding pocket of ERβ with amino acids G305, A346 and H475 (Fig. 1A). Treatment with E2 during 1 hour of ERβ-transfected HEK cells induced phosphorylation of ERK that disappeared after transfection with an ERβ in which the amino acids E305/A346/H475 were all replaced by alanine (triple mutant ERβ, tmERβ) (Fig. 1B). We obtained the same result when replacing E305 by alanine (single mutant E305A ERβ, smERβ) (Fig. S2A).

Docking model indicates that BPA also forms hydrogen bonds with E305 and H475 (Fig.1A). BPA treatment during one hour increased ERK phosphorylation in HEK cells transfected with ERβ, producing an effect at concentrations within the pico-molar range similar to E2 (Fig. 1C). Cells transfected with tmERβ (Fig. 1C) did not show increased ERK phosphorylation by BPA. The same results were observed in cells transfected with the smERβ (Fig. S2B). Neither E2 nor BPA produced a significant increase in ERK phosphorylation in untransfected HEK cells after 1 hour of treatment (Fig. S2C and S2D). The fact that not only the triple mutant but also the single mutant abrogates the rapid phosphorylation of ERK points to an essential role of these residue, and suggest that E2 and BPA may behave as orthosteric ligands, binding to the same active site of ERβ.

To study the nuclear-initiated pathway we used the transactivation assay in HELN ERβ reporter cells (*22*). E2 activated the nuclear pathway with an EC50 of 68 pM while BPA activated the nuclear pathway with an EC50 of 351 nM (Fig. 1D). The observed affinity of the receptor population for BPA presented and IC50 of 523 nM relative to the binding of E2 (Fig. 1E).

The results described above indicated that E2 had high affinity, binding potently to ERβ and activating both the nuclear and extranuclear initiated pathways with high efficacy.

BPA, however, bound to ERβ with low affinity, but had very high efficacy in activating the extranuclear pathway and very low efficacy in activating the nuclear pathway. These differences in the efficacy of BPA suggest the existence of two mechanisms: one to initiate the extranuclear pathway, which is weakly affinity dependent, and another to initiate the nuclear pathway, which is strongly affinity dependent.

BPA but not d_{16}-BPA initiated extranuclear ERβ activation of ERK

To gain mechanistic insights into how BPA increases its efficacy in activating the ERβ-initiated extranuclear pathway we decided to use two different deuterated BPA molecules. d_{16}-BPA, a molecule identical to BPA but in which all hydrogen atoms have been exchanged for deuterium, and d_{14}-BPA in which the exchangeable hydrogens in the phenolic oxygens are ^{1}H instead of ^{2}H. Both d_{16}-BPA and d_{14}-BPA were commercial and were identified by NMR and HPLC-MS/MS (Fig. S3, Fig. S4 and Fig. S5).

The change of ^{1}H by ^{2}H completely cancelled rapid BPA-induced ERK phosphorylation in HEK transfected with ERβ (Fig. 1F) while d_{14}-BPA had a similar effect as BPA (Fig. 1G). This indicated that the ^{1}H in the phenolic group are needed for the extranuclear pathway activation. Then, we sought to study the nuclear pathway, d_{16}-BPA presented a similar transactivation activity compared to BPA and d_{14}-BPA (Fig. 1D), and the observed binding affinity was slightly higher to that of BPA (BPA IC50=244 nM; d_{16}-BPA IC50=99 nM) (Fig. 1E). This small change in affinity could be due to altered strength of the hydrogen bonding upon deuteration, known as the Ubbelohde effect (*23*). In conclusion, the potency and efficacy of the nuclear-initiated action was identical among BPA and its two deuterated isotopologues, yet the extranuclear pathway depend on the hydroxyl groups and their deuteration suppresses the biological effect.

The large difference we observed in the effects of d_{16}-BPA and d_{14}-BPA (Fig. 1F and G) implies a large isotopic effect involving an ionization reaction, probably a proton transfer. No obvious carbon-hydrogen bond can be broken and if the isotopic effect is observed, it must be due to proton transfer from hydroxyl groups. This is supported by the effect of d_{14}-BPA that all its hydrogens are substituted by deuterium except those bound to phenolic oxygens, and it caused ERK phosphorylation equal to that of BPA (Fig. 1G).

The different effects between d_{16}-BPA and d_{14}-BPA suggest that, although deuterium-hydrogen back-exchange occurs at the hydroxyl groups, this happens at a slow rate. To

verify this experimentally, we decided to study by HPLC-MS/MS how much d_{16}-BPA in the protein-free culture medium was transformed into d_{14}-BPA at 1 hour and at 24 hours. These are the times at which the experiments were performed, 1-hour incubations for the western blots and between 16 and 24 hours for the rest of the experiments. After a 1-hour dilution in culture medium, we found that 85% of the initial d_{16}-BPA remained unchanged and after 24 hours, more than 60% of the initial d_{16}-BPA remained unchanged (Fig. S6A). These results indicated that the back-exchange of ^{2}H for ^{1}H was slow in the culture medium, buffered at pH=7.4, giving that BPA is slightly alkaline (pKa of BPA=9.6-11.3) (*24*). In conclusion, the hydroxyls of d_{16}-BPA remained deuterated in a high proportion during the time of the experiments.

BPA but not d_{16}-BPA initiated extranuclear ERα activation of ERK

To study if the same mechanism activated the extranuclear ERα-initiated pathway we transiently transfected HEK cells with ERα. More than 65% of the cells expressed ERα, and its location was mostly nuclear or perinuclear (Fig. S1C and S1D). In these cells, we found that E2 and BPA increased ERK activation in a dose dependent manner while d_{16}-BPA was without effect (Fig. 2 A-C). Binding to ERα was identical between BPA and d_{16}-BPA (Fig. 2D) and transactivation in HELN ERα reporter cells was similar between BPA and d_{16}-BPA, although with a much lower efficacy than E2 (Fig. 2E). These experiments suggest that a similar mechanism works for the extranuclear activation of ERK by BPA binding to ERα.

DPN but not d_2-DPN induced ERβ activation of ERK

To analyze if other ER ligands behave as BPA we chosen the specific ERβ agonist diarylpropionitrile (DPN) (*25*) which in docking model forms hydrogen bonds with G305, H475 and A346 within the ligand binding domain of ERβ (not shown). Competitive ligand binding experiments in HELN ERβ reporter cells shows an affinity for ERβ within the nanomolar range (IC50=4.3 nM) (Fig. 3B). The deuterated molecule d_2-DPN, synthesized by $^{2}H/^{1}H$ exchange and identified by HPLC-MS/MS (Fig. S6B and 6C), which had deuterated hydroxyls, presented a similar binding to that of DPN (IC50=3.1 nM) (Fig. 3A). The transactivation assay demonstrated that the nuclear-initiated pathway was equally potent for DPN and d_2-DPN (Fig. 3B). DPN was able to phosphorylate ERK (Fig. 3C and 3D), yet the hydroxyl deuterated DPN molecule (d_2-DPN) was without effect (Fig. 3E and 3F). Deuterated DPN was stable during one hour in culture medium and

more than 90% still deuterated (Fig. S6D). After 24 hours more than 50% of it remained deuterated (Fig. S6D).

These experiments suggested that a proton transfer was also involved in DPN activation of the extranuclear ERβ-initiated pathway.

Rapid actions of d_{16}-BPA and d_2-DPN on pancreatic β-cells

To study whether the same mechanism was present in mouse cells expressing native ER, we performed the experiment described in Fig. 4A. We obtained pancreatic β-cells from male mice and record the activity of ATP-sensitive K^+ (K_{ATP}) channels using the patch-clamp technique in the cell-attached mode. Mouse and human β-cells express both ER (*17, 26*). Acute treatment with BPA decreases K_{ATP} channel activity with a high efficacy in mice and human β-cells in an ERβ-dependent manner (*18, 27*). This effect occurs within minutes and it is, therefore, independent of gene transcription. We demonstrated that 1nM BPA almost completely reduced K_{ATP} channel activity, yet 1nM d_{16}-BPA had no effect (Fig. 4B and 4D). When we carried out the same experiment but using DPN instead of BPA, we found a similar result, the d_2-DPN molecule produced no effect on K_{ATP} activity while DPN almost fully abolished K_{ATP} activity (Fig. 4C and 4E).

These experiments suggest that in the rapid regulation of K_{ATP} channels in mouse β-cells also involves a proton transfer from these ligands.

Differential ERβ activation of extranuclear signaling pathways by E2 and BPA isotopologues

The experiments described so far strongly indicated that a proton transfer from BPA and DPN activated, with high efficacy, the ERβ-dependent phosphorylation of ERK. This mechanism is expected to switch other extranuclear signaling pathways and therefore, we decided to study the interactome obtained from immunoprecipitation of ERβ HEK cells combined with proteomics in the absence of ligand (vehicle) and in the presence of E2, BPA, d_{16}-BPA and d_{14}-BPA (Fig. 5A). We identified a total of 1039 proteins and screened for nonspecific binding by comparing the sample with the anti-ERβ antibody to a sample using IGG. In this way we selected 279 proteins interacting with ERβ. We performed a functional pathway enrichment analysis using the gene ontology database of biological processes as well as Reactome and Cytoscape software, revealing the activation of a variety of signaling pathways after 1 hour (Fig. S7A). We observed proteins directly related to ERβ, including those involved in ER signaling, cell cycle and cell death, folding

proteins and endoplasmic reticulum stress (Fig. S7A and Table S1). In order to analyze the protein interaction pattern per each treatment as a whole, we performed a principal component analysis (PCA) plot of the interacting protein profile detailed in Table S2. The PCA showed a differentiated population between BPA and d_{14}-BPA compared to d_{16}-BPA (Fig. 5B). BPA and d_{14}-BPA showed a similar population, whereas that of d_{16}-BPA was more similar to that obtained with vehicle (Fig. 5B). The population shown by E2 was different from that of BPA and d_{16}-BPA. (Fig. 5B).

Fig. 5C shows a heatmap of the abundance of proteins that immunoprecipitate together with ERβ in the presence of vehicle, E2, BPA, d_{14}-BPA and d_{16}-BPA. In the presence of vehicle there are a large number of proteins already interacting with ERβ. When we applied E2 we observed that some of the ERβ-interacting proteins increased or decreased interaction in a similar pattern, although not identical to BPA. The d_{16}-BPA has little or no effect and its pattern is similar to that of vehicle while d_{14}-BPA presented a similar pattern to that of BPA (Fig. 5C). These data can also be plotted as a graph of the relative abundance of proteins against the different stimuli (Fig. 5D), showing how vehicle and d_{16}-BPA cluster together, and BPA clusters with d_{14}-BPA while E2 is in between.

The overall view of the pattern with the different ligands illustrated how the result in the case of most proteins is compatible with the proton transfer mechanism suggested.

We next performed western blotting of the ERβ immunoprecipitation using antibodies against HPA5, CAT, JUN, ERK and CDK1 (Fig. 5E) which confirmed the results described in Fig. 5C and 5D.

This experiment suggests that the ERβ switch activated by proton transfer from BPA, interacts with a large group of extranuclear signaling proteins involved in key cellular processes.

DISCUSSION

Our results show that the endocrine disruptor BPA binds to both ER with low affinity and activates nuclear actions at concentrations close to its affinity. However, it initiates the extranuclear pathway with high efficacy, at concentrations up to 1000 times lower than its affinity. Experiments with BPA and the ERβ ligand DPN, both deuterated, show a strong kinetic isotope effect. The greater mass of ^{2}H compared with ^{1}H results in a lower vibrational frequency which results in a lower zero-point energy for the C-^{2}H or O-^{2}H bonds compared to C-^{1}H or O-^{1}H bonds and as a consequence, a higher activation energy required for reaching the transition state for bond cleavage. Therefore, it results in lower

reaction rates for the deuterated analogues when the rate-determining step involves the cleavage of a covalent C-^{1}H/^{2}H or O-^{1}H/^{2}H bond (*20*). Thus, the lack of effect of deuterated ligands points to a proton transfer from those ligands, specifically from phenol hydroxyls, as a mechanism for switching the extranuclear pathway. This mechanism shows a high efficacy in activating the extranuclear pathway and is much less affinity-dependent than the one activating the nuclear pathway.

Recently synthesized PaPE ligands, including the BPA-based PaPE-4 have the ability to interact with ERs to preferentially activate the extranuclear pathway. The reasoning behind is that low affinity ligands require only the input of a triggering signal from the ER-hormone complex to initiate a kinase cascade rather than a more sustained action of the ER-hormone complex to recruit coactivators and the entire transcriptional machinery as occurs with the nuclear pathway (*9*). Similar reasoning could apply to BPA.

It is not well understood at the molecular level how ligands, including BPA, bind to and dissociate from ERs, nor how these dynamics affect the subsequent activation of signaling cascades. In the case of ER ligands, it is known that the decrease in the equilibrium dissociation constant (K_D) is due to an increase in the kinetic dissociation constant (k_{off}) while the kinetic association constant (k_{on}) remains practically unchanged (*28*). For BPA the k_{on}=1.3x10^6 M^{-1}s^{-1}, exactly the same as for E2, thus both display a fast association rate constant and both ligands likely recognize the same conformation of the receptor (*28*). The rate of dissociation is however very different, the k_{off}= 0.27 s^{-1} for BPA and 1.2 10^{-3} s^{-1} for E2, thus BPA dissociates more rapidly than E2 giving BPA a weaker affinity for ERβ (*28*). The difference in the dissociation rates gives a much lower half-life of the ER-ligand complex for BPA than E2, BPA dissociates from the receptor in seconds while E2 is in the range of several minutes. The k_{off} is directly related with the half-life ($t_{1/2}$) of the receptor-ligand complex, $t_{1/2}$=ln2/k_{off} (*29*). In the case of BPA with a k_{off}=0.27 s^{-1}, $t_{1/2}$ of the ERβ-BPA complex is 2.6 s, which must be enough for a proton transfer reaction to occur. Proton transfer is one of the fastest reactions in chemistry. Activation of the GPCR, rhodopsin, which involves proton transfer reactions, occurs in a few milliseconds (*30*). Thus, the ERβ-BPA complex should remain long enough for a proton transfer process to occur and trigger a conformational change that activates the extranuclear pathway.

Rapid proton transfer signaling has been demonstrated in G protein-coupled receptors (GPCRs), including rhodopsin, adrenergic and muscarinic receptors (*31-33*). Activation of rhodopsin, involves two key chemical reactions, a retinal photoisomerization and a

proton transfer reaction from a retinal Schiff base to a counterion glutamate residue (*31, 34*) . In this way, rhodopsin functions as a molecular off/on switch, being fully inactive in the dark and to rapidly switch to a fully active structure in the light. It is possible, therefore, that ERs function similarly in response to ligands with the appropriate chemical properties to produce proton transfer, such as BPA. After binding, the receptor will convert to an active conformation due to proton transfer from the ligand acting as donor to an acceptor within the ligand binding domain. The hydroxyl groups of the ligands, BPA, DPN and E2 form H-bonds with aminoacids E305 and H475 in the case of ERβ and E535 or H524 in the case of ERα (*22*), making possible the coupling between ligands and acceptors for a ground-state proton transfer reaction (*35*). It is possible, therefore, that ligand binding functions as a molecular off/on switch for extranuclear ER-mediated actions, which would explain the high efficacy of this process triggered at doses far below K_D in the case of BPA.

Signaling proteins interacting with ERβ will respond to the active conformation switched by proton transfer, initiating an array of signaling pathways involved in estrogen signaling, cell division and death, endoplasmic reticulum stress and others. Extranuclear signaling by nuclear receptors is a complex phenomenon which is less understood at the molecular level than the nuclear one. The activation of such extranuclear pathways by ligands other than E2, such as endocrine-disrupting chemicals has been understudied (*36, 37*). Extranuclear ER interact with a plethora of signaling proteins associated to the plasma membrane or present in the cytosol, such as G proteins and other receptors and kinases involved in extranuclear-initiated signaling triggered by estrogens (*4*). The nuclear interactomes of activated ER are relatively well know (*38*), however the extranuclear interactome in the absence and presence of ligands is very much unknown. We found in the interaction proteomics experiment that in the absence of added ligands, ERβ constitutively binds an abundant amount of proteins, in agreement with published results in MCF7 cells (*39*). The interaction map of ERβ changes in a similar direction in the presence of BPA and d_{14}-BPA, however d_{16}-BPA produced very little change. Therefore, the overall interaction map of ERβ should be activated by the proposed proton transfer reaction, probably producing a subsequent conformational change responsible for activation of these signaling pathways. This indicates that this mechanism switches the entire spectrum of extranuclear signaling pathways initiated by ERβ.

The fact that, in addition to BPA, the ERβ-specific ligand DPN initiates the extranuclear actions through the proton transfer mechanism suggests that the natural hormone E2 could behave in the same way. Technical problems have not allowed us to synthesize an E2 with deuterated hydroxyls and although we can speculate that the natural hormone might use this same mechanism, we have not been able to verify this directly.

We propose that BPA and DPN activate the extranuclear-initiated ERβ signaling after a proton transfer reaction from the hydroxyls to an acceptor group, likely E305 and/or H475. This proton transfer will induce a conformational change that will activate a variety of signaling pathways involved in essential cellular processes. This mechanism should work also to activate ERα extranuclear signaling pathways and could be extended to other ligands and nuclear receptors.

The work reported here should have an impact on the understanding of estrogen receptor function. It should help to better design new drugs specific for the nuclear and extranuclear pathways. It should also have an impact on the identification of endocrine disrupting chemicals, which is currently based on the shape of ligands and their interaction with receptors, basically considering K_D, but does not consider a chemical reaction as a switch to activate estrogen receptors and thus a mechanism that does not rely exclusively on affinity.

MATERIALS AND METHODS

Chemical reagents

17β-estradiol CAS number: 50-28-2 (Sigma-Aldrich, Madrid, Spain), 4,4'-(propano-2,2-diil)difenol (BPA) CAS number: 80-05-7 (Sigma-Aldrich, Madrid, Spain), d_{16}-BPA CAS number: 80-05-7 (Cambridge Isotope Laboratories, Massachusetts, USA), d_{14}-BPA CAS number: 80-05-7 (Polymer Source Inc, Canada), 2,3-bis(4-Hydroxyphenyl)-propionitrile (DPN) CAS number:1428-67-7 (Tocris, Madrid, Spain) and collagenase (Sigma-Aldrich, Madrid, Spain). Bisphenols and E2 were dissolved in DMSO (Sigma-Aldrich, Madrid, Spain).

Cell culture and transfection protocol

HEK cells were kindly provided by Dr. Asia Fernandez (IDiBE-UMH). Cells were cultured with Dulbecco's modified Eagle's medi um (DMEM) containing 4.5 g/L glucose

and 4 mM L-glutamine (DMEM, Gibco, ref: 11965092) supplemented with 10%FBS (Cultek, Spain), penicillin (100 U/ml), streptomycin (100 µg/ml) and finally incubated under humid atmosphere at 37°C in 5% CO_2. Subsequently, cells were seeded under different conditions, as required by the assay, with different treatments, using DMEM supplemented. Transfection was performed according to the supplier's instructions, using Lipofectamine 2000 reagent (Invitrogen, ref: 11668-027) and medium supplemented with 2% FBS without antibiotics. A total of 10^5 cells per well were added to 24-well plates and, after 24 hours, transfected with the following plasmids as required for the experiment: mTFP-Reporter (Rep) teal fluorescent protein plasmid, ERα plasmid (ERα), ERβ plasmid (ERβ), Triple mutant plasmid (tmERβ) or single mutant plasmid (smERβ); all at a concentration of 300ng/well for 48 hours. Transfection efficiency was determined by western blot and immunofluorescence. After recovery time, cells were treated with the different compounds (E2, BPA, d_{14}-BPA and d_{16}-BPA) at different concentrations specified in each figure. For treatment conditions, HEK cells were cultured with phenol red-free DMEM (Gibco, ref: 21063029) supplemented with 5% FBS devoid of charcoal (Gibco, ref: 12676-029) during treatment.

To characterize the ERα and ERβ activities of BPA and DPN analogues, we used already established HELN hERα and HELN hERβ reporter cell lines (Grimaldi et al., 2019). Briefly, HELN hERα and HELN hERβ were obtained by stable expression of hERα and hERβ in HELN (HeLa ERE-βglobin-luciferase) cells. HELN ER cells were cultured in Dulbecco's Modified Eagle Medium: Nutrient Mixture F-12 (DMEM/F-12) without phenol red and 1 g/L glucose and supplemented with 5% stripped fetal bovine serum, 100 units/mL of penicillin, 100 µg/mL of streptomycin, 0.5 µg/mL puromycin and 1 mg/mL geneticin in a 5% CO2 humidified atmosphere at 37°C.

Animals, islet culture and dispersed islet cells

All adult male mice were maintained under standard housing conditions (12 h light/dark cycle, ad libitum feeding). The mice were killed and islets were isolated as previously described (*40*). For patch-clamp experiments, islets were dispersed into single cells and plated on coverslips as previously described (*41*). Cells were maintained at 37°C in a humidified atmosphere of 95% O_2 and 5% CO_2 and 48 hours of culture were used. Experimental procedures were carried out in accordance with Royal Degree 1201/2005 and the European Directive 2010/63/EU. The ethical committee of the Miguel Hernández

University reviewed and approved the methods used (approvals ID: UMH.IDI.AN.01.20).

Western blot assay

Cells were cultured and lysed with Laemmli buffer. Proteins were separated by SDS-PAGE and then transferred to a PVDF membrane (*26, 42*). The membranes were blocked with 5% milk, washed with TBST and incubated with primary antibodies overnight. Primary antibody used in these experiments were: ERα (ref: MA5-13191, Invitrogen, 1:1000); ERβ (ref: MA5-24807, Invitrogen, 1:1000); pERK (ref: 4370S, Cell Signalling, 1:1000); ERK total (ref: 4696S, Cell Signalling, 1:2000); β-actin (ref: 5316, Sigma, 1:5000); GAPDH (ref: 5174, Cell signalling, 1:1000) The membranes were then washed three times with TBST, and incubated with secondary antibodies for 1 h. The secondary antibodies used were: Goat Anti-mouse (ref: 1706516, BIORAD, 1:5000) or Goat Anti-rabbit (ref: 1706515, BIORAD, 1:5000). The membranes were incubated with SUPERSIGNAL West Femto reagent (Thermofisher, ref: 34096), and the protein bands were detected and visualised using a transilluminator kit (Bio-Rad, Hercules, CA, USA). The intensities of the bands were quantified by scanning densitometry (Un-SCAN software, MA, USA).

Synthesis of d_2-DPN

The synthesis of d_2-DPN was carried out from commercial DPN. First, DPN obtained from TOCRIS (Bristol, UK; Ref: 1494) was dissolved in deuterated DMSO (SIGMA-Merck, Ref: 103591) with 0.1 equivalent of HCl. Deuterium were introduced through a reaction with D_2O at 50°C and sonication for 25 minutes. After this time, samples were kept in a hot bath for 2 hours at 80ºC and finally, the samples were lyophilised and dry stored until use.

Determination of BPA and DPN isotopologues by HPLC-MS/MS

Liquid chromatography LC-MS/MS equipped with a diode array detector (DAD) and coupled to a triple quadrupole mass spectrometer Shimadzu LCMS-8050 were used to analyse the samples of interest. Samples (10 µL) were injected through an autosampler, separated on an Agilent Zorbax ODS column (150 mm × 3 mm, 5 µm) at 30°C and detected by DAD (UV 214 nm). The flow rate was set at 0.3 mL /min with methanol and water as mobile phase. The linear gradient started isocratic at 50% methanol for 3 min,

then increased to 90% in 7 min and 100% in another 8 min and was maintained for another 2 min, then the gradient returned to 50% methanol in 2 min and was maintained for 5 min. The mass spectrometer was operated in ESI-negative mode, using multiple reaction monitoring mode for quantification. Nitrogen was used as a cover gas and auxiliary gas. The gas temperature was 350°C, the nebuliser was 40 psi, the gas flow was 10 L/min, and the capillary was 4500 V. Data were analysed using Qualitative Analysis B.06.00 software (Agilent, CA, USA) (*43*).

Identification of BPA isotopologues by NMR

^{1}H-NMR spectra were recorded on a Bruker AVANCE 500 spectrometer Bruker AC-300, ARX-300 and AV-400 instrument. Chemical shifts (δ) are reported in ppm and referenced to d_6-DMSO (2.50ppm) (*44*). All of the NMR spectra were recorded in d_6-DMSO at 293 K.

Patch Clamp recordings

K_{ATP} channel activity was recorded using standard patch-clamp recording procedures from isolated β-cells as described previously (*41, 45*). Around 80–90% of the single cells were identified as β-cells by their response to high glucose, consisting in action currents in cell-attached configuration. Currents were recorded using an Axopatch 200B patch-clamp amplifier (Axon Instruments Co. CA, USA). Patch pipettes were pulled from borosilicate capillaries (Sutter Instruments Co. CA, USA) using a flaming/brown micropipette puller P-97 (Sutter Instruments Co. CA, USA) with resistance 3-5 MΩ when filled with the pipette solutions as specified below. Bath solution contained (in mM): 5 KCl, 135 NaCl, 2.5 CaCl2, 10 HEPES and 1.1 MgCl2 (pH 7.4) and supplemented with glucose as indicated. The pipette solution contained (in mM): 140 KCl, 1 MgCl2, 10 HEPES and 1 EGTA (pH 7.2). The pipette potential was held at 0 mV throughout recording. K_{ATP} channel activity was quantified by digitizing 60 s sections of the current record, filtered at 1 kHz, sampled at 10 kHz by a Digidata 1550B (Molecular Devices Co.0 CA, USA), and calculating the mean open probability of the channel (NP_o) during the sweep. Channel activity was defined as the product of N, the number of functional channels, and P_o, the open-state probability. P_o was determined by dividing the total time channels spent in the open state by the total sample time. Experiments were carried out at 36°C.

Transactivation assays

The cells were seeded in white 96 well plates (Greiner CellStar) with a density of 25000 cells per well in assay growth media. Cells were incubated for 24 h at 37°C and 5% CO2, then the media was decanted and replaced with the sample serially diluted in phenol red free DMEM/F-12 with 5% dextran coated charcoal stripped FBS and 1% penicillin/streptomycin. The maximum solvent concentration was 0.1%. Samples were incubated for a further 16 h to 24 h at 37°C at 5% CO2. After the exposure period, the test media was decanted and replaced with test media containing 0.3 mM luciferin. Luminescence, expressed as relative light units (RLU), was measured using a PerkinElmer MicroBeta luminometer. All samples were run in quadruplicate per plate and were run in at least two independent experiments.

Competitive binding assays

HELN ERα and HELN ERβ cells were seeded in white 96 well plates with clear bottom (Greiner CellStar) with a density of 75000 cells per well in assay growth media. The cells were incubated for 24 h at 37°C and 5% CO2, then the media was decanted and replaced with the sample serially diluted in the media and tritiated reference ligand (0.1 nM E2). The maximum solvent concentration was 0.1%. The samples were incubated for a further 2 h at 37°C at 5% CO2. After the exposure period, unbound material was aspirated and the cells were washed three times with cold PBS. After visual inspection to check the good condition of the cells, 100 μL of LSC cocktail (Emulsifier-Safe, Packard Bioscience) were added and plates were agitated for 5 min. Bound radioactivity values were expressed in disintegrations per minute (dpm). Results were plotted as the percentage of radioactivity (in dpm) versus the concentration of the unlabeled reference compound (M) or water samples. All samples were run in quadruplicate per plate and were run in at least two independent experiments.

Immunofluorescence assay

HEK cells transfected with ERα or ERβ as appropriate were fixed with 4% paraformaldehyde (SIGMA, ref: 1635) in PBS for 15 min, then permeabilised with 0.2% Triton X-100 (Sigma, Ref: T8787) for 10 min and blocked with 5% BSA (CAPRICORN, Cat: BSA-1T) in PBS for 1 hr. Antibodies for rabbit ERα (Invitrogen, Ref: MA5-14501, 1:200) and mouse ERβ (thermoficher, ref: MA1-23217, 1:200) were used, followed by secondary anti-rabbit Alexa Flour 488 (Termofisher, ref: A32723, 1:1000) and anti-

mouse Alexa fluor 567 (Termofisher, ref: A32740, 1:1000) antibodies. As negative controls, the samples were incubated with the secondary antibodies without primary antibodies. Finally, the nuclei of the cells were stained with DAPI (SIGMA, ref: DUO82040). Cells were observed using a Zeiss Confocal LSM900 microscope equipped with a camera (Zeiss-Vision, Munich, Germany), and images were acquired at x63 magnification and analysed using ZEN software (version 3.2; Zeiss-Vision, Munich, Germany).

Co-immunoprecipitation assay.

Immunoprecipitation was performed according to the protocol described previously (*26*). HEK293 cells were seeded in 6-well plates at a density of 10^6 cells/well and transfected with 2µg of ERβ plasmid and were treated with different compounds (Vehicle, E2, BPA, d_{14}-BPA and d_{16}-BPA) at the concentration of 1nM for 1 hour. After treatment, HEK293 cells were lysed with immunoprecipitation buffer (50 mM Tris, pH 7.5, 4 mM NaCl, 2 mM MgCl2, 10 mM NaF, 1 mM PMSF, 1% Triton X-100 and Complete Protease inhibitor mixture, Roche Diagnostics) for 45 min on ice and centrifuged at 20000g for 10 min at 4ºC. They were then cleaned with Protein-G-Dynabeads magnetic beads (Thermo scientific, Cat. No 53139) for 1 h at 4°C to remove non-specific binding proteins. After removal of the protein-G beads, the same amount of protein lysates was incubated with antibodies for ERβ (Invitrogen, Ref: MA5-24807), overnight, while mouse IgG (Cell signalling, Ref: 2729S) was used as a negative control. After incubation, inmunoprecipitated were washed and resuspended with Laemmli buffer. The immunoprecipitated proteins were analysed by proteomics and western blotting.

The antibodies used in western blots of this experiment were: HSPA5 (ref: PA1-014A, Invitrogen, Massachuset, USA, 1:1000); CAT (ref: 12980S, Cell Signalling, 1:1000), CDK1 (ref: ab133327, Abcam, 1:1000); JUN (ref: 9165S, Cell Signalling, 1:1000); ERK (ref: 4696S, cell Signalling, 1:2000); IGG (ref: 2729S, Cell Signalling, 1:5000)

S-Trap™ digestion for proteomics

Each sample was diluted with lysis buffer to 5% sodium dodecyl sulfate (SDS) and 25 mM triethylammonium bicarbonate (TEAB). Samples were reduced and alkylated by adding 5 mM tris(2-carboxyethyl)phosphine (TCEP) and 10 mM chloroacetamide (CAA) for 30 minutes at 60ºC.

Protein digestion in the S-Trap filter (Protifi, Huntington, NY, USA) was performed following the manufacturer's instructions with minor changes (*46*). Each sample was digested at 37°C overnight using a trypsin:protein ratio of 1:15 and was cleaned with a StageTip C18 prior to LC-ESI-MS/MS analysis.

Liquid chromatography and mass spectrometry analysis (LC-ESI-MS/MS) for proteomics

After desalting, peptide concentration was measured by Qubit™ Fluorometric Quantitation (Thermo Fisher Scientific). Half of each digested sample was subjected to 1D-nano LC ESI-MS/MS (Liquid Chromatography Electrospray Ionization Tandem Mass Spectrometric) analysis using an Ultimate 3000 nano HPLC system (Thermo Fisher Scientific) coupled online to a Orbitrap Exploris 240 mass spectrometer (Thermo Fisher Scientific). Peptides were eluted onto a 50 cm × 75 µm Easy-spray PepMap C18 analytical column at 45°C and were separated at a flow rate of 250 nL/min using a 90 min gradient ranging from 2 % to 95 % mobile phase B (mobile phase A: 0.1% formic acid (FA); mobile phase B: 100 % acetonitrile (ACN), 0.1 % FA).

Data acquisition was performed using a data-dependent top-20 method, in full-scan positive mode, scanning 350 to 1200 m/z. Survey scans were acquired at a resolution of 60,000 at m/z 200, with Normalized Automatic Gain Control (AGC) target (%) of 300 and a maximum injection time (IT) of 40 ms. The top 20 most intense ions from each MS1 scan were selected and fragmented via Higher-energy collisional dissociation (HCD). Resolution for HCD spectra was set to 45,000 at m/z 200, with AGC target of 200 and maximum ion injection time of 120 ms. Isolation of precursors was performed with a window of 1 m/z, exclusion duration (s) of 10 and the HCD collision energy was 32. Precursor ions with single, unassigned, or six and higher charge states from fragmentation selection were excluded.

Proteomics data analysis and sequence search

Raw instrument files were processed using Proteome Discoverer (PD) version 2.5.0.400 (Thermo Fisher Scientific). MS2 spectra were searched using Mascot Server v2.8.0 (Matrix Science, London, UK) and a target/decoy database built from sequences in the Homo sapiens proteome at Uniprot Knowledgebase (20230420). All searches were configured with dynamic modifications for pyrrolidone from Q (-17.027 Da) and oxidation of methionine residues (+15.9949 Da) and static modification as

carbamidomethyl (+57.021 Da) on cysteine, monoisotopic masses, and trypsin cleavage (max 2 missed cleavages). The peptide precursor mass tolerance was 10 ppm, and MS/MS tolerance was 0.02 Da. The false discovery rate (FDR) for proteins, peptides, and peptide spectral matches (PSMs) peptides were kept at 1%.

Pathways enrichment analysis

Enrichment pathway analysis was performed using Cytoscape version 3.9.1 with ClueGO version 2.5.9 (*47*) and CluePedia version 1.5.0 (*48*) plugins. GO Biological Process databases were used and those with a P-value <=0.05 were considered as threshold values. The model organism Homo sapiens was used for ClueGO analyses. Principal component analysis (PCA) and clustering of relative protein abundance by treatment was performed using ClustVis software (https://biit.cs. ut.ee/clustvis/) (*49*).

Molecular modelling

Structures available in the Protein Data Bank have been used for both human LBD-ERα and ERβ, where the protein and E2 or BPA are co-crystallized, 2OCF, 3UU7 and 5TOA, respectively. These structures contained unresolved residues in mobile regions of the protein that diffracted poorly, the missing amino acids were reconstructed after generation of a homology model in the Swiss-Model server (*50*). In addition, a molecular docking technique was performed to generate the structure of LBD-ERβ with BPA within the LBD cavity, using YASARA Structure v22.5.22 software (*18, 26*). The ligand-protein interactions have been detected with the Protein-Ligand Interaction Profiler (FLIP) algorithm (*51*). The figure has been prepared with PyMol Software (Schrödinger, L. & DeLano, W., 2020. PyMOL, Available at: http://www.pymol.org/pymol).

Statistical analysis

The GraphPad Prism 8.0 software (GraphPad Sofware, Inc., CA, USA) was used for all statistical analyses. Detailed information on the statistical analysis performed in each case, including replicates, as well as the number of times the experiments were repeated, is given in the figure legends. Data are expressed as mean±SEM. To assess differences between working groups, paired t-test or one-way analysis of variance (ANOVA) was used where appropriate. A probability level ≤0.05 was considered statistically significant. P-values are indicated in the text or in the figure legends.

REFERENCES AND NOTES

1. C. J. Gruber, W. Tschugguel, C. Schneeberger, J. C. Huber, Production and actions of estrogens. *N Engl J Med* **346**, 340-352 (2002).
2. J. M. Hall, D. P. McDonnell, Coregulators in nuclear estrogen receptor action: from concept to therapeutic targeting. *Mol Interv* **5**, 343-357 (2005).
3. P. Ascenzi, A. Bocedi, M. Marino, Structure-function relationship of estrogen receptor alpha and beta: impact on human health. *Mol Aspects Med* **27**, 299-402 (2006).
4. E. R. Levin, S. R. Hammes, Nuclear receptors outside the nucleus: extranuclear signalling by steroid receptors. *Nat Rev Mol Cell Biol* **17**, 783-797 (2016).
5. A. Pedram *et al.*, Developmental phenotype of a membrane only estrogen receptor alpha (MOER) mouse. *J Biol Chem* **284**, 3488-3495 (2009).
6. A. Pedram *et al.*, Estrogen reduces lipid content in the liver exclusively from membrane receptor signaling. *Sci Signal* **6**, ra36 (2013).
7. M. Adlanmerini *et al.*, Mutation of the palmitoylation site of estrogen receptor alpha in vivo reveals tissue-specific roles for membrane versus nuclear actions. *Proc Natl Acad Sci U S A* **111**, E283-290 (2014).
8. A. Abot *et al.*, The uterine and vascular actions of estetrol delineate a distinctive profile of estrogen receptor alpha modulation, uncoupling nuclear and membrane activation. *EMBO Mol Med* **6**, 1328-1346 (2014).
9. Z. Madak-Erdogan *et al.*, Design of pathway preferential estrogens that provide beneficial metabolic and vascular effects without stimulating reproductive tissues. *Sci Signal* **9**, ra53 (2016).
10. P. Yi *et al.*, Structural and Functional Impacts of ER Coactivator Sequential Recruitment. *Mol Cell* **67**, 733-743 e734 (2017).
11. G. G. Kuiper *et al.*, Interaction of estrogenic chemicals and phytoestrogens with estrogen receptor beta. *Endocrinology* **139**, 4252-4263 (1998).
12. J. M. Molina-Molina *et al.*, In vitro study on the agonistic and antagonistic activities of bisphenol-S and other bisphenol-A congeners and derivatives via nuclear receptors. *Toxicol Appl Pharmacol* **272**, 127-136 (2013).
13. L. N. Vandenberg, C. M. Schaeberle, B. S. Rubin, C. Sonnenschein, A. M. Soto, The male mammary gland: a target for the xenoestrogen bisphenol A. *Reprod Toxicol* **37**, 15-23 (2013).
14. M. Susiarjo, T. J. Hassold, E. Freeman, P. A. Hunt, Bisphenol A exposure in utero disrupts early oogenesis in the mouse. *PLoS Genet* **3**, e5 (2007).
15. L. Speroni *et al.*, New insights into fetal mammary gland morphogenesis: differential effects of natural and environmental estrogens. *Sci Rep* **7**, 40806 (2017).
16. Y. J. Jeng, C. S. Watson, Combinations of physiologic estrogens with xenoestrogens alter ERK phosphorylation profiles in rat pituitary cells. *Environ Health Perspect* **119**, 104-112 (2011).
17. P. Alonso-Magdalena *et al.*, Pancreatic insulin content regulation by the estrogen receptor ER alpha. *PLoS One* **3**, e2069 (2008).
18. L. Marroqui *et al.*, Bisphenol-S and Bisphenol-F alter mouse pancreatic beta-cell ion channel expression and activity and insulin release through an estrogen receptor ERbeta mediated pathway. *Chemosphere* **265**, 129051 (2021).
19. R. M. C. Di Martino, B. D. Maxwell, T. Pirali, Deuterium in drug discovery: progress, opportunities and challenges. *Nat Rev Drug Discov* **22**, 562-584 (2023).
20. J. Atzrodt, V. Derdau, W. J. Kerr, M. Reid, Deuterium- and Tritium-Labelled Compounds: Applications in the Life Sciences. *Angew Chem Int Ed Engl* **57**, 1758-1784 (2018).
21. F. H. Westheimer, The Magnitude of the Primary Kinetic Isotope Effect for Compounds of Hydrogen and Deuterium. *Chemical Reviews* **61**, 265-273 (1961).

22. V. Delfosse *et al.*, Structural and mechanistic insights into bisphenols action provide guidelines for risk assessment and discovery of bisphenol A substitutes. *Proc Natl Acad Sci U S A* **109**, 14930-14935 (2012).
23. M. Krzan, J. Keuschler, J. Mavri, R. Vianello, Relevance of Hydrogen Bonds for the Histamine H2 Receptor-Ligand Interactions: A Lesson from Deuteration. *Biomolecules* **10**, (2020).
24. G. Zeng *et al.*, Adsorption behavior of bisphenol A on sediments in Xiangjiang River, Central-south China. *Chemosphere* **65**, 1490-1499 (2006).
25. M. J. Meyers *et al.*, Estrogen receptor-beta potency-selective ligands: structure-activity relationship studies of diarylpropionitriles and their acetylene and polar analogues. *J Med Chem* **44**, 4230-4251 (2001).
26. I. Babiloni-Chust *et al.*, G protein-coupled estrogen receptor activation by bisphenol-A disrupts the protection from apoptosis conferred by the estrogen receptors ERalpha and ERbeta in pancreatic beta cells. *Environ Int* **164**, 107250 (2022).
27. S. Soriano *et al.*, Rapid insulinotropic action of low doses of bisphenol-A on mouse and human islets of Langerhans: role of estrogen receptor beta. *PLoS One* **7**, e31109 (2012).
28. R. L. Rich *et al.*, Kinetic analysis of estrogen receptor/ligand interactions. *Proc Natl Acad Sci U S A* **99**, 8562-8567 (2002).
29. J. Corzo, Time, the forgotten dimension of ligand binding teaching. *Biochem Mol Biol Educ* **34**, 413-416 (2006).
30. B. Knierim, K. P. Hofmann, O. P. Ernst, W. L. Hubbell, Sequence of late molecular events in the activation of rhodopsin. *Proc Natl Acad Sci U S A* **104**, 20290-20295 (2007).
31. C. K. Meyer *et al.*, Signaling states of rhodopsin. Retinal provides a scaffold for activating proton transfer switches. *J Biol Chem* **275**, 19713-19718 (2000).
32. A. Scheer, F. Fanelli, T. Costa, P. G. De Benedetti, S. Cotecchia, The activation process of the alpha1B-adrenergic receptor: potential role of protonation and hydrophobicity of a highly conserved aspartate. *Proc Natl Acad Sci U S A* **94**, 808-813 (1997).
33. W. A. Timms D, Kelly DR, Broadley KJ, Davies RH Ligand-activated trans-membrane proton transfer in beta 1-adrenergic and m2-muscarinic receptors. *Recept Channels* **2**, 107-119 (1994).
34. Y. Mizuno, K. Katayama, H. Imai, H. Kandori, Early Proton Transfer Reaction in a Primate Blue-Sensitive Visual Pigment. *Biochemistry* **61**, 2698-2708 (2022).
35. A. P. Demchenko, Proton transfer reactions: From photochemistry to biochemistry and bioenergetics. *BBA Adv* **3**, 100085 (2023).
36. F. Acconcia, V. Pallottini, M. Marino, Molecular Mechanisms of Action of BPA. *Dose Response* **13**, 1559325815610582 (2015).
37. A. Nadal *et al.*, Extranuclear-initiated estrogenic actions of endocrine disrupting chemicals: Is there toxicology beyond paracelsus? *J Steroid Biochem Mol Biol* **176**, 16-22 (2018).
38. G. Nassa *et al.*, A large set of estrogen receptor beta-interacting proteins identified by tandem affinity purification in hormone-responsive human breast cancer cell nuclei. *Proteomics* **11**, 159-165 (2011).
39. C. Stellato *et al.*, Identification of cytoplasmic proteins interacting with unliganded estrogen receptor alpha and beta in human breast cancer cells. *Proteomics* **15**, 1801-1807 (2015).
40. A. Nadal, B. Soria, Glucose metabolism regulates cytosolic Ca2+ in the pancreatic beta-cell by three different mechanisms. *Adv Exp Med Biol* **426**, 235-243 (1997).
41. M. Valdeolmillos, A. Nadal, D. Contreras, B. Soria, The relationship between glucose-induced K+ATP channel closure and the rise in [Ca2+]i in single mouse pancreatic beta-cells. *J Physiol* **455**, 173-186 (1992).

42. W. Thangnipon *et al.*, Protective role of N-trans-feruloyltyramine against beta-amyloid peptide-induced neurotoxicity in rat cultured cortical neurons. *Neurosci Lett* **513**, 229-232 (2012).
43. A. Liu *et al.*, High-performance thin-layer chromatography coupled with HPLC-DAD/HPLC-MS/MS for simultaneous determination of bisphenol A and nine brominated analogs in biological samples. *Anal Bioanal Chem* **411**, 725-734 (2019).
44. A. J. M. M. Gregory R. Fulmer, Nathaniel H. Sherden, Hugo E. Gottlieb, Abraham Nudelman, Brian M. Stoltz, John E. Bercaw, and Karen I. Goldberg, NMR Chemical Shifts of Trace Impurities: Common Laboratory Solvents, Organics, and Gases in Deuterated Solvents Relevant to the Organometallic Chemist. *Organometallics* **29**, 2176–2179 (2010).
45. J. Martinez-Pinna *et al.*, Oestrogen receptor beta mediates the actions of bisphenol-A on ion channel expression in mouse pancreatic beta cells. *Diabetologia* **62**, 1667-1680 (2019).
46. S. Ciordia *et al.*, Digging deeper into bile proteome. *J Proteomics* **230**, 103984 (2021).
47. G. Bindea *et al.*, ClueGO: a Cytoscape plug-in to decipher functionally grouped gene ontology and pathway annotation networks. *Bioinformatics* **25**, 1091-1093 (2009).
48. G. Bindea, J. Galon, B. Mlecnik, CluePedia Cytoscape plugin: pathway insights using integrated experimental and in silico data. *Bioinformatics* **29**, 661-663 (2013).
49. T. Metsalu, J. Vilo, ClustVis: a web tool for visualizing clustering of multivariate data using Principal Component Analysis and heatmap. *Nucleic Acids Res* **43**, W566-570 (2015).
50. M. Biasini *et al.*, SWISS-MODEL: modelling protein tertiary and quaternary structure using evolutionary information. *Nucleic Acids Res* **42**, W252-258 (2014).
51. S. Salentin, S. Schreiber, V. J. Haupt, M. F. Adasme, M. Schroeder, PLIP: fully automated protein-ligand interaction profiler. *Nucleic Acids Res* **43**, W443-447 (2015).

Funding sources

This work was supported by Ministerio de Ciencia e Innovación, Agencia Estatal de Investigación (AEI) grant PID2020-117294RB-I00 (AN, JM-P), PID2020-117569RA-I00 and CNS2022-135505 (LM), European Union's Horizon 2020 research and innovation programme under grant agreement GOLIATH No. 825489 (AN) and PROMETEO II/2020/006 (AN). CIBERDEM is an initiative of the Instituto de Salud Carlos III.

Acknowledgements

The authors thank Beatriz Bonmati Botella, Maria Luisa Navarro, and Salomé Ramon for their excellent technical assistance. We thank Dr. J.A. Encinar (IDiBE-UMH) for docking simulations. Workflow schemes in figures 4 and 5 were performed with BioRender.

Author contributions

AN: conceived the study, designed experiments, acquired funds, and oversaw the project. JM-P, PB acquired funds, designed and performed experiments and analyzed data. RM-G, JM-P, LM, MG, SC, SS designed and performed experiments and analyzed data. AN. wrote the manuscript. All authors participated in reviewing and editing of the manuscript.

Conflicts of Interest

The authors declare no conflict of interest.

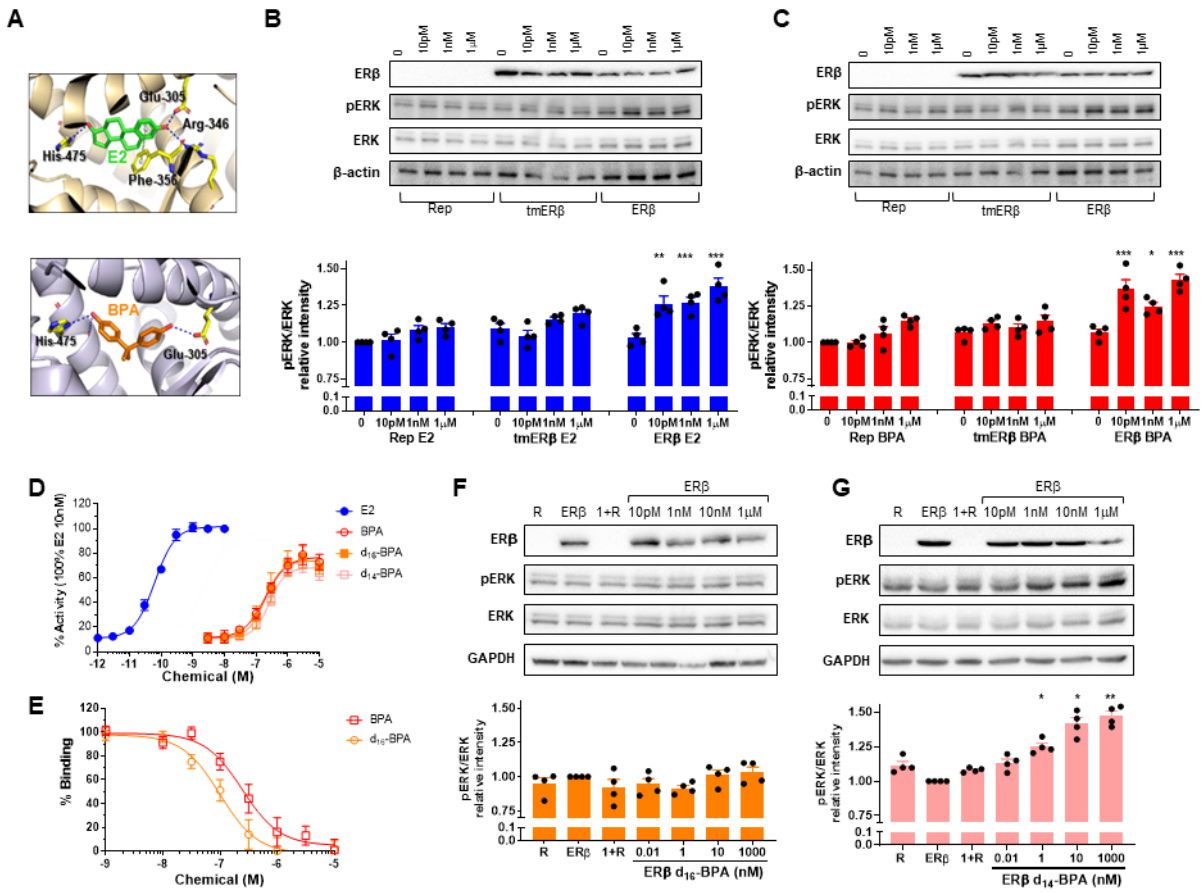

Fig. 1. Activation of the extra-nuclear pathway in HEK cells transfected with ERβ.
(**A**) Interaction of E2 (upper panel) with G305, A346 and H475, and of BPA (lower panel) with G305 and H475 within the ligand binding site of ERβ. Amino acids involved in H-bonds are marked with a blue dashed line. (**B** and **C**) HEK cells transfected with the reporter plasmid (Rep), the ERβ triple mutant (tmERβ) or ERβ, were treated with E2 in B or BPA in C, at the indicated concentrations for 1 hour. Top part shows representative immunoblots of ERβ, pERK, ERK, and β-actin expression. Activation values of pERK were quantified against ERK and are shown as graphs (low). (**D**) Luciferase assay in HELN ERβ reporter cells. Cells were treated with E2, BPA, d_{16}-BPA and d_{14}-BPA for 16 hours at the indicated concentrations. The maximal luciferase activity (100%) was obtained with 10 nM E2. Data are represented as the percentage of maximal E2 induction. Values are the mean±SEM from 3 separated experiments. (**E**) Competitive inhibition of [^{3}H]-E2 binding to hERβ by BPA and d_{16}-BPA. HELN ERβ cells were incubated with different concentrations of BPA and d_{16}-BPA in the presence of 0.1 nM E2 [^{3}H]-E2 during 16 hours. Data are represented as the percentage of maximal [^{3}H]-E2 binding. Values are the mean±SEM from 3 separated experiments. (**F** and **G**) HEK cells transfected with reporter plasmid labeled as R, or ERβ were treated with d_{16}-BPA or d_{14}-BPA at the indicated concentrations for 1 hour. Top part shows representative immunoblot of ERβ expression, pERK, ERK and GAPDH. ERK phosphorylation was quantified against total ERK (low). Data are shown as mean±SEM of 4 separated experiments. *P < 0.05, **P < 0.01, ***P < 0.001. One way ANOVA followed by Tukey test. Note that the column labelled as ERβ represents cells transfected with ERβ plus 0.00002% DMSO used as a control.

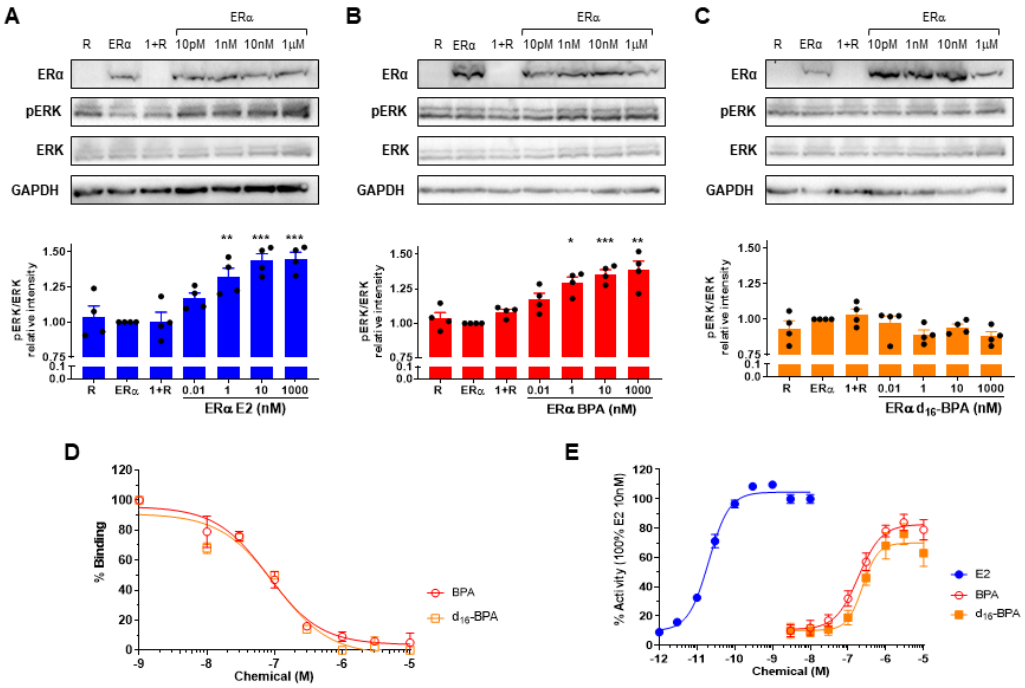

Fig.2. ERK activation in HEK cells transfected with ERα.
(**A-C**) Representative immunoblots of ERα, pERK, ERK and GAPDH (top), and quantification of pERK versus ERK (bottom) in response to vehicle (DMSO, indicated as ERα), E2, BPA and d_{16}-BPA for 1 hour in HEK cells transfected with either reporter (Rep or R) or ERα plasmids. Results are expressed as mean±SEM from 4 separated experiments. *P < 0.05, **P < 0.01, ***P < 0.001, One-way ANOVA followed by Tukey test. (**D**) Luciferase assay in HELN ERα reporter cells. Cells were treated with E2, BPA and d_{16}-BPA for 16 hours at the indicated concentrations. The maximal luciferase activity (100%) was obtained with 10 nM E2. Data are represented as the percentage of maximal E2 induction. Values are the mean±SEM from 3 separated experiments. (**E**) Competitive inhibition of [^{3}H]-E2 binding to hERα by BPA and d_{16}-BPA. HELN ERα cells were incubated with different concentrations of BPA and d_{16}-BPA in the presence of 0.1nM E2 [^{3}H]-E2 during 16 hours. Data are represented as the percentage of maximal [^{3}H]-E2 binding. Values are the mean±SEM from 3 separated experiments.

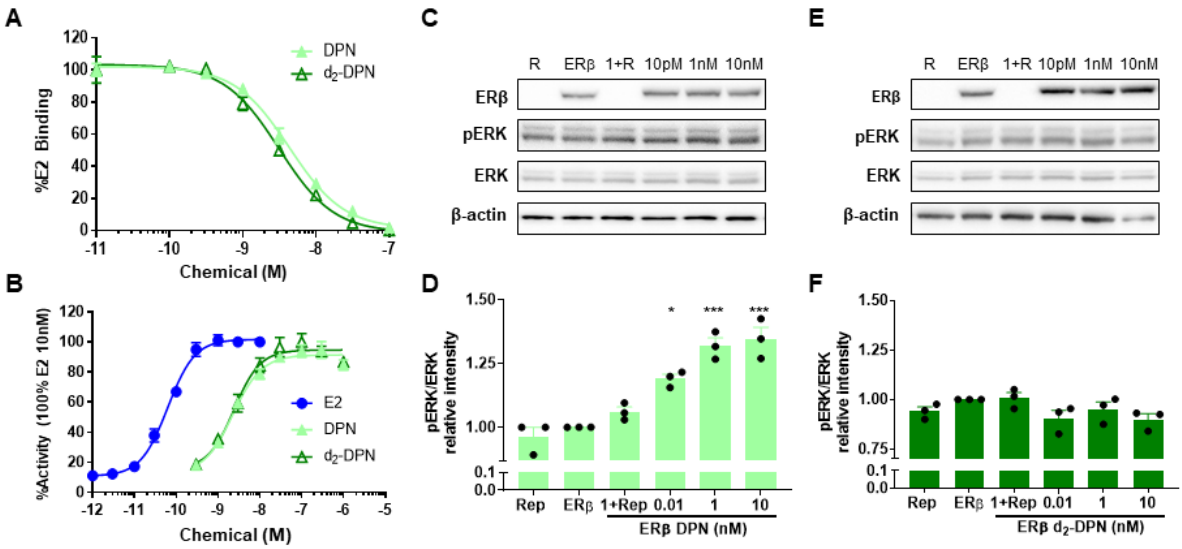

Fig. 3. Effect of DPN in the ERK activation in HEK cells transfected with ERβ.
(**A**) Competitive inhibition of [^{3}H]-E2 binding to hERβ by DPN and d_2-DPN. HELN ERβ cells were incubated with different concentrations of DPN and d_2-DPN in the presence of 0.1nM nM E2 [^{3}H]-E2 during 16 hours. Values are represented as mean±SEM from 3 separated experiments. (**B**) Luciferase assay in in HELN ERβ reporter cells. Cells were treated with E2, DPN and d_2-DPN for 16 hours at the indicated concentrations. The maximal luciferase activity (100%) was obtained with 10 nM E2. Data are represented as the percentage of maximal E2 induction. Values are the mean±SEM from 3 separated experiments. (**C** and **D**) HEK cells were transfected with reporter (R) or ERβ plasmid and treated with DPN at 10pM, 1nM, 10nM and 1µM concentrations for 1 hour. Representative immunoblots are shown of ERβ, ERK and β-actin expression as well as pERK phosphorylation. In the low part, graphs showing the quantification of pERK expressed as the ratio pERK/ERK relative intensity. (**E** and **F**) The same as in C and D but treating the cells with d_2-DPN. *P < 0.05, **P < 0.01, ***P < 0.001, One-way ANOVA followed by Tukey test, n=3 separated experiments.

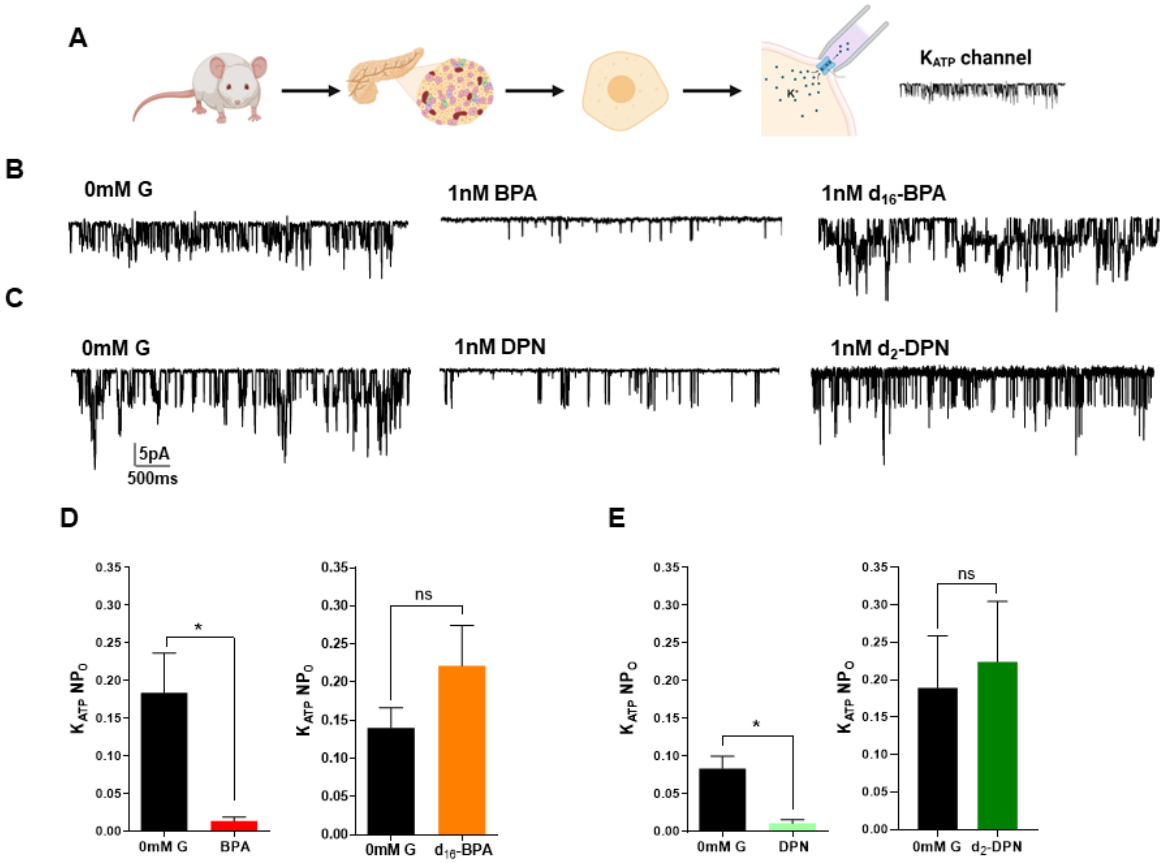

Fig.4. Regulation of K_{ATP} channel activity in pancreatic β-cells.
(**A**) Scheme illustrating the experimental workflow to study the acute effect of BPA, d_{16}-BPA, DPN and d_2-DPN on the activity of K_{ATP} channels. (**B**) Representative recordings of K_{ATP} channel activity in 0 mM glucose (left), 10 min after application of 1 nM BPA (middle) or 1 nM d_{16}-BPA (right). (**C**) Representative recordings of K_{ATP} channel activity in 0 mM glucose (left), 10 min after application of 1 nM DPN (middle) or 1 nM d_2-DPN (right). (**D**) Average mean open probability of K_{ATP} channels elicited by 0 mM glucose and in the presence of 1 nM BPA (left, 8 cells) or 1 nM d_{16}-BPA (right, 8 cells). (**E**). Average mean open probability of K_{ATP} channels elicited by 0 mM glucose and in the presence of 1 nM DPN (left, 4 cells) or 1 nM d_2-DPN (right, 8 cells). * $p<0.05$, ns: non-significant, paired t-test.

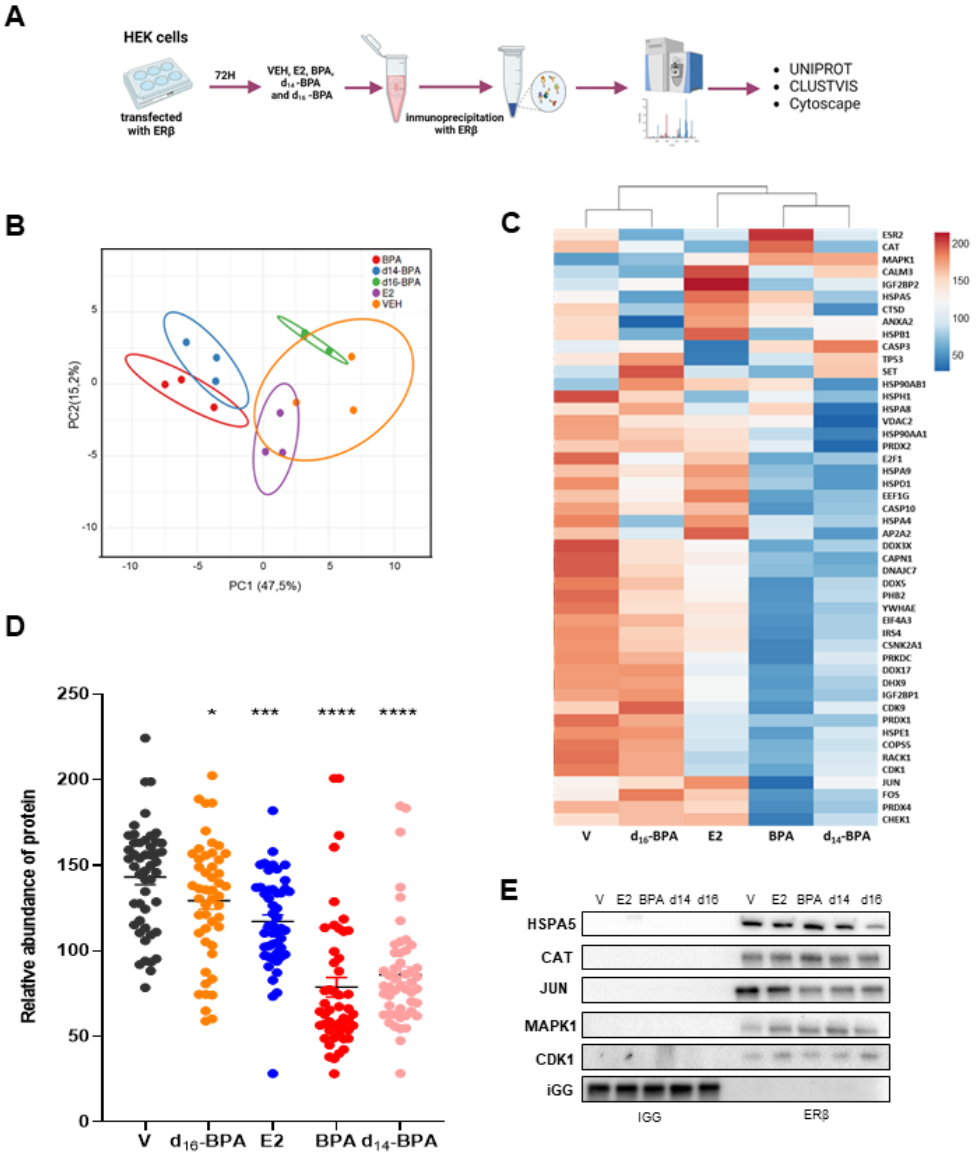

Figure 5. Changes in the ERβ interactome in response to E2, BPA, d_{14}-BPA and d_{16}-BPA.
(**A**) Summary of the experimental workflow applied to identify ERβ-interacting proteins: ERβ-transfected HEK cells were subjected to different treatments, vehicle (0.00002% DMSO, indicated as V), E2, BPA, d_{14}-BPA and d_{16}-BPA at a concentration of 1 nM for 1 hour, and then immunoprecipitated with an anti-ERβ antibody, to identify ERβ-interacting proteins by proteomics. (**B**) Principal component plot (PCA) of ERβ interactome assessment in ERβ-transfected HEK cells treated with V, E2, BPA, d_{14}-BPA and d_{16}-BPA for 1 hour. Graph was developed using relative abundances of proteins identified by proteomics. (**C**) Heat map of molecular signatures showing the relative abundance of 49 proteins directly linked to ERβ. The heatmap data matrix visualizes the values in the cells using a color gradient that gives an overview of the largest and smallest values in the matrix. The cluster lines at the top show the grouping by treatment. (**D**) Graph of relative protein abundances showing the independent behavior of each treatment. One-way ANOVA followed by Dunn test was performed showing significant differences between groups, *$P < 0.05$, ***$P < 0.001$, ****$P < 0.0001$. (**E**) Immunoblots of representative proteins interacting with ERβ. The proteins were evaluated in immunoprecipitates of IGG or with ERβ, in the different treatments performed (V, E2, BPA d_{14}-BPA and d_{16}-BPA) for 1 hour.